Sensing self-assembled alkanethiols by differential transmission interrogation with terahertz metamaterials

Xiaojun Wu,[1] Baogang Quan,[1] Xuecong Pan,[1] Xinlong Xu,[1,2,*] Xinchao Lu,[3] Xiaoxiang Xia,[1] Junjie Li,[1] Changzhi Gu,[1] and Li Wang[1]

[1]Beijing National Laboratory for Condensed Matter Physics and Institute of Physics, Chinese Academy of Sciences, Beijing 100190, China

[2]Nanobiophotonic Center, State Key Laboratory for Incubation Base of Photoelectric Technology and Functional Materials, and Institute of Photonics & Photon-Technology, Northwest University, Xi'an 710069, China

[3]Institute of Microelectronics, Chinese Academy of Sciences, Beijing 100029, China

*Corresponding author: xlxuphy@nwu.edu.cn

Received 12 April 2013; revised 1 June 2013; accepted 4 June 2013; posted 10 June 2013 (Doc. ID 188702); published 5 July 2013

Surface-enhanced electromagnetic response in the resonant regions of split-ring resonators offers a sensitive way to probe the surface dipoles formed by alkanethiol molecules with a terahertz wave by a differential transmission (DT) interrogation method. The DT signal mainly comes from the interaction between alkanethiols and metamaterials by electron transfer and/or the variation of the dielectric constant. The Lorentz model is used to demonstrate the principle of DT interrogation theoretically, which suggests the variation of both frequency and damping of resonance can be captured cooperatively. This method has been employed to experimentally demonstrate the sensing feasibility for the chain length dependence of the alkanethiol molecules. Numerical simulations confirm that the enhancement is large at the gap and corner regions of this kind of metamaterials.

OCIS codes: (300.6495) Spectroscopy, terahertz; (160.3918) Metamaterials; (130.6010) Sensors.
http://dx.doi.org/10.1364/AO.52.004877

1. Introduction

Label-free molecular sensing, especially molecules with specific interactions, are of fundamental importance for chemical analysis, medical diagnosis, environmental protection, and so on. Optics-based label-free sensing methods such as surface plasmon resonance (SPR) with metallic films [1] and localized surface plasmon resonance [2] with metallic nanoparticles offer powerful sensing platforms for effective and practical bio/chemical applications. These methods are based on the intensity and/or the resonant frequency change due to the interaction of electromagnetic waves with the microenvironments. How to further improve the flexibility and tunability of this interaction is of significant importance for the application and manipulation of these sensors effectively.

Recently, with the concept of effective permittivity (ε) and/or permeability (μ) engineering, metamaterials are thought to provide the opportunity to enhance the manipulation of electromagnetic response with the properties that may not be readily available in nature. This emergent field offers another promising platform for sensing with the characteristics of designable and tunable resonant features [3]. A higher degree of design freedom is enabled compared with the conventional SPR sensors [4]. The figure-of-merit of metamaterials can be enhanced by the pattern

1559-128X/13/204877-07$15.00/0

design and engineering of the light coupling [5]. In the roadmap of metamaterial applications as stated by Zheludev [6], sensing applications will be one of the next pleasant prospects in metamaterials.

Proof-of-principle studies of sensing based on metamaterials have been demonstrated in sensing water [7], dielectric film, specific molecules [8], DNA, protein, and so on, from the microwave region [9–11], through the terahertz (THz) region [12], to the infrared-visible region [13–16]. Meanwhile, recently reported metamaterials-inspired THz waveguide geometries have also been demonstrated to significantly improve the sensitivity because of the enhanced THz response near the resonant region [17,18]. In these studies, the resonant frequency (wavelength) shift and/or intensity change interrogations with metamaterials are usually employed to evaluate the sensitivity of the sensors. These interrogation methods can capture either the frequency shift or damp constant variation of the resonance. For example, many investigations based on the aforementioned methods have been conducted including DNA sensing using split-ring resonators (SRRs) in the microwave region by Lee *et al.* [11,19], protein detection in the THz region by Yoshida *et al.* [20], permeability tunability with silicon nanospheres by Driscoll *et al.* [21], flexible metamaterial for thiol sensing by Xu *et al.* [13], paper metamaterials for urea sensing by Tao *et al.* [22], and ultrasensitive Fano-resonant metamaterials [23–25] for molecular monolayers by Wu *et al.* [26]. Even though the field started, sensing with metamaterials [27–29] is still in its infancy, in particular, effective data analysis and more sensitive sensing methods are in high demand.

In this paper, we propose an analysis method based on THz metamaterials to understand the principle of differential transmission (DT) interrogation more systematically. Compared with the aforementioned data analysis methods which monitor either the resonant frequency shift or intensity change, our method can extract the peak–valley difference (ΔPV) including the variation of both frequency and damping of resonance cooperatively in DT curve and in turn the ΔPV is used as the sensing signal. Surface dipoles formed by alkanethiol molecules interact with metamaterials in the format of electron transfer and/or the change of the microenvironmental dielectric constant, which mainly introduces a DT change in the resonant regions. The Lorentz model as a symmetric resonant response is employed to theoretically demonstrate the DT interrogation in THz metamaterials. All the characteristics of the dispersive shape change due to the frequency shift and/or damping constant change of metamaterials can be captured by ΔPV. Theoretical analysis shows that ΔPV is approximately linear with the central frequency (f_c) shift and the resonant damping constant (Γ), which is desirable for the sensing application. Experimental results demonstrate that the ΔPV signal has the capability to resolve the chain length of alkanethiol molecules with different carbon numbers. Numerical simulations also confirm that the enhancement is large at the gap and corner regions of this kind of metamaterials.

2. Simulation

Numerical calculation using the finite integral technique is employed to simulate the electromagnetic response of the metamaterials with the format of SRRs. In the simulation, periodic boundary conditions were considered and transient solver was applied. The hexahedral mesh was used and the thickness for both the gold film of the SRRs and the single layer of molecules linked on the gold film were 80 and 10 nm, respectively. We employed the perfect electrical conductor for gold in the simulation and its conductivity tended to infinity. The designed size of the unit cell is similar to our previous pattern design [30] with the following parameters: unit cell 43 μm, period 55 μm, width of the line 4 μm, and the gap 4 μm. The substrate is silicon with the dielectric constant of 11.7. The photography of our designed SRRs is shown in Fig. 1(a). To model analyte layers, a thin layer of self-assembled molecules [schematically shown in Fig. 1(b)] was chosen as an effective microenvironmental permittivity of 1.2. Due to the computational complexity, the self-assembled molecules linked on the U-shaped gold SRRs were treated as a layer of 100 nm in thickness. Although the calculation cannot capture the charge transfer between the metal and molecules, it can

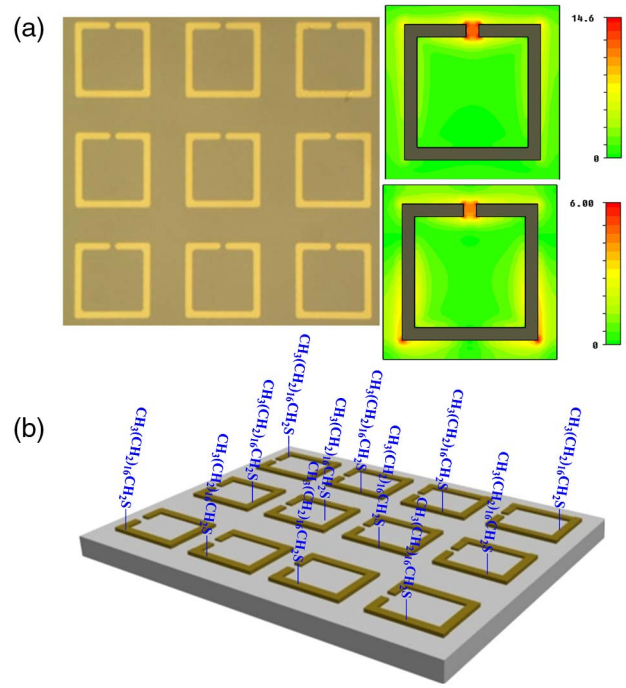

Fig. 1. (a) Photography of the U-shaped SRRs metamaterials with the parameters stated in the main text. Simulated near-field amplitude distribution around a SRR for Mode 1 (top right) and Mode 2 (bottom right). (b) Schematics of alkanethiol molecules with $CH_3(CH_2)_{17}SH$ can form a self-assembled monolayer when they interact with gold (Au).

provide the key physical properties of the electromagnetic response and the near-field enhancement information in the THz region [31]. Figure 2(a) demonstrates the calculated transmission spectra of pristine SRRs (red squares) and the SRRs with the analyte layer. In the calculation, the THz wave is polarized along the gap side of SRRs. One mode near 0.4 THz (Mode 1) and one mode near 1.2 THz (Mode 2) are observed, which is consistent with our previous observation [32]. Mode 1 can be explained by a combination of capacitance and inductance (LC resonance), which is mainly due to the coupling of electric and magnetic responses in SRRs. Therefore, Mode 1 has an electric dipole moment parallel to the open gap and a magnetic dipole moment orthogonal to the ring. However, with regard to Mode 2, it may stem from the standing pattern along the length of the ring, which can be approximately described by a dipole resonant frequency. It is not evident that the intensity change or resonant frequency shift of the monolayer-modified spectra compared with the pristine spectrum. However, the DT spectrum [blue line in Fig. 2(a)] unveils the change in the resonant regions. Here, the DT spectrum is defined as $((T_{\mathrm{modi}} - T_{\mathrm{pri}})/T_{\mathrm{pri}}$, which is the difference between the pristine and the modified SRRs spectra. It is evident that Mode 1 and Mode 2 show different sensitivity, which suggests different original electromagnetic response. Near-field electrical field mapping for Mode 1 [Fig. 1(a) top right] and Mode 2 [Fig. 1(a) bottom right] also show different distributions. For example, the electrical field is strongly localized and confined in the gap region for Mode 1, while the field expands along every arm of the SRR unit with three strong areas in the gap and corners for Mode 2. To give an estimation of the enhancement in the gap region, we demonstrate the calculated near-field spectrum in the SRRs gap as shown in Fig. 2(b). It is suggested that much stronger electrical enhancement is located in the resonant region.

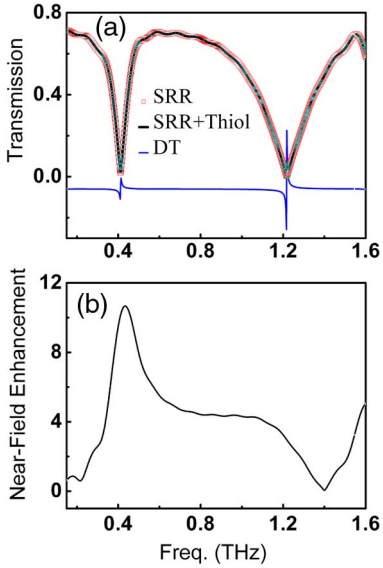

Fig. 2. (a) Calculated electromagnetic response (red squares) of SRRs with Mode 1 near 0.4 THz and Mode 2 near 1.2 THz. The electromagnetic response has been tuned when alkanethiol molecules (C18) bond to the SRRs (black line). The DT signal is shown in the bottom panel with the blue line (value offset by 0.06 for clarity). (b) Calculated near-field amplitude enhancement spectrum near the SRRs gap.

3. Theoretical Consideration for Differential Transmission Integration

Even though differential methods such as differential extinction [33] and differential reflection [26] have been used to give the "Yes" or "No" answers to molecular interaction, the intrinsic correlation of signals to f_c and Γ is limited. The meaning for the differential interrogation is still obscure, even if it is used in practice in [26] and [33]. A Lorentz model can be used for the analysis quantitatively in Fig. 3, which can be written as follows:

$$T = T_0 - \frac{2A}{\pi}\frac{\Gamma}{4(f - f_c)^2 + \Gamma^2}, \tag{1}$$

where T_0 is the background of the transmission and A is the spectral weight calculated from the amplitude distribution of the resonant region. The resonant curve is shown in the inset in Fig. 3 with $f_c = 1.236$ THz for electric mode. The background transmission will influence only the baseline of the DT spectrum. However, without consideration of the baseline shift, the differential function of Eq. (1) can be simplified as:

$$\frac{dT}{T} \approx \frac{8(f - f_c)df_c + \left(\frac{4(f-f_c)^2}{\Gamma} - \Gamma\right)d\Gamma}{4(f - f_c)^2 + \Gamma^2}. \tag{2}$$

This suggests that under small deviation approximation, DT is approximately linear with the shift of f_c and the change of Γ. Figure 3 (black line) demonstrates DT as a function of frequency with f_c redshifted by 0.0001 THz. It is obvious that the redshift of f_c introduces a dispersive odd symmetry shape of DT signal with two lobes, in which the first one is negative and the second is positive. Meanwhile, the blueshift of f_c introduces the opposite polarity (not shown here). On the other hand, increasing Γ by 0.0001 introduces one positive lobe (red line in Fig. 3) with an even symmetry and

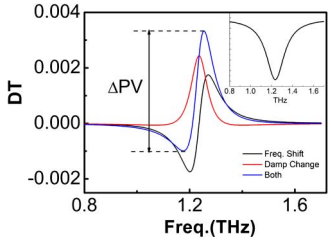

Fig. 3. DT spectroscopy due to the central frequency change (black curve), damp change (red curve), and both (blue curve). The peak–valley value (ΔPV) near the resonant region is demonstrated. The inset is a Lorentz resonator at 1.236 THz.

decreasing Γ brings a negative lobe. Usually, in sensing experiments, the adsorption of molecules on the sensing surface will cause a redshift of f_c and/or an increase of Γ [19–22]. As a combination of two effects, the DT shape is asymmetric as shown in Fig. 3 (blue line). The polarity of the DT signal would be useful for the simplification of sensing information.

We define the peak–valley value by ΔPV as demonstrated in Fig. 3 as a parameter to evaluate the change of both f_c and Γ, quantitatively. Figure 4 gives the contour map of the DT signal with the spontaneous change of both f_c and Γ. The contour line is an ellipse with the longitudinal axis along f_c. It suggests that the variation of f_c will dominate in the DT signal. If one of them (f_c or Γ) is smaller than the other one or both of the changes are small, the DT change would be approximately linear with f_c or Γ. The cross section of the contour map (dash line) in Fig. 4 shows the case when Γ is fixing. The bottom panel in Fig. 4 demonstrates that the ΔPV changes linearly with f_c (black curve). It is similar to Γ (not shown). There are some benefits for this peak–valley definition for DT interrogation. First, if the laser drifts a little, it can only shift the baseline of the DT spectrum. However, the ΔPV definition does not depend on the baseline (as shown in Fig. 3) and it has the capability to some extent to minimize the influence from laser drift. Second, it evaluates both f_c and Γ changes due to their linear relationship under the small signal approximation. Third, the ΔPV signal is amplified in the resonant regions, which is a benefit for small change in sensing applications.

4. Sample Preparation and Experimental Setup

Our metamaterials in the format of SRRs [shown in Fig. 1(a)] were fabricated by traditional microfabrication methods, involving the processes of photolithography, electron beam evaporation, lift-off, and so on. To ensure the surface clean, oxygen plasma (PVA TePla, PS210, for 10 min under the power of 600 W) is used to remove all possible organic materials on the metamaterials.

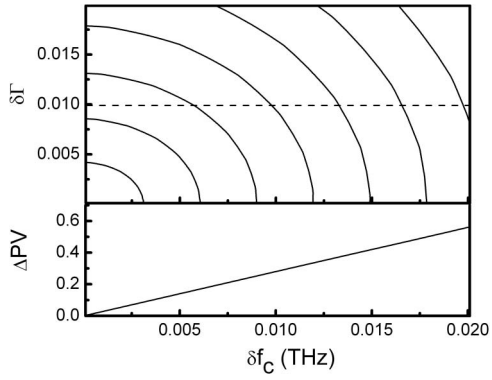

Fig. 4. Contour map of the sensor characteristic with the spontaneous change of both central frequency and damp. The dash line is a cross section when the damp constant is fixed and the contour line is demonstrated in the bottom panel with the linear dependence of ΔPV value with the change of central frequency.

The alkanethiol molecule $CH_3(CH_2)_nSH$ (n stands for different carbon number) can have a specific chemical interaction with the Au surface. They can form well-ordered, covalent bonded monolayers and tailor the metamaterial surface chemical properties selectively [34]. This affords a playground for not only applications such as molecular electronics [35] and lithography [36], but also fundamental property tests [34].

The Au-based metamaterial surface is functionalized via specific thiol chemical interaction to form a monolayer of thiol-terminated molecules as shown in Fig. 1(b). The alkanethiol molecules are uniformly covalently bond to the metal area and the remaining nonimmobilized substance was washed way after deposition. Alkanethiol molecules of $CH_3(CH_2)_nSH$ ($n = 1$, 5, 11, and 17) with different carbon numbers are chosen. The molecules were bought from Sigma-Aldrich without further purification and 7 mM alkanethiol solution in ethanol were prepared. The alkanethiol interacts with the gold surface quickly with high-sticking probability and reaches saturation in 10 min. The saturation increases with the raise of the CH_2-molecule, and the stabilization of the transition state is by ~0.65 kJ/mol per CH_2 [37]. To get the uniform and stable layers on the surface of metamaterials, the metamaterials have been immersed into the alkanethiol solution for more than 11 h with the same condition for different alkanethiol molecules to ensure the dynamical balance of the reaction. The SRRs were then dried with nitrogen gas. Following these procedures, the alkanethiol self-assembled monolayers are well-ordered, tightly bonded, and highly densed, which provides a simple motif for selective tailoring of surface chemical properties [34]. After each experiment, the surface of the same SRRs was cleaned by oxygen plasma to remove all possible organic materials on the metamaterials. The control experiment was also following the aforementioned procedures by immersing the SRRs in liquid ethanol for 11 h and then drying them with nitrogen gas. Our home-built THz time-domain spectroscopy [8,38] setup is based on the generation from a low-temperature-grown GaAs photoconductivity antenna integrated with a silicon hemisphere and the ZnTe crystal detection of the THz pulse radiation, which can be found in our previous work [8,39]. The measurements have been done on the system purged with dry nitrogen to avoid the strong influence of the water vapor in the ambient. As for the discussion of the noise influence to the THz transmission spectroscopy, the system noise will affect the measured results. The dynamic range, defined as the maximum value of the THz signal divided by the maximum of the background noise, for our employed system can approach 10,000.

5. Experimental Results and Discussion

Figure 5 (black line) demonstrates the original SRRs transmission spectra with THz polarization along with the gap side of SRRs at normal incidence. Mode

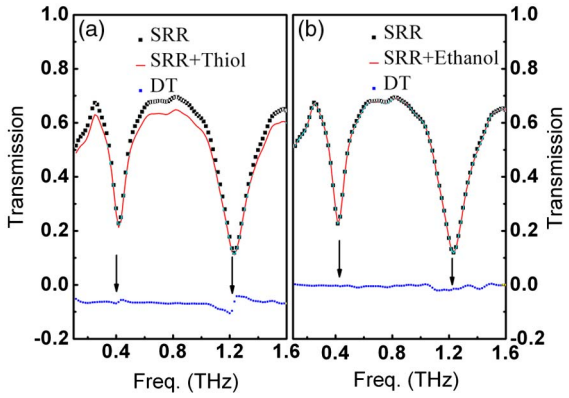

Fig. 5. Original metamaterial electromagnetic response (black line) with Mode 1 near 0.4 THz and Mode 2 near 1.2 THz. (a) The electromagnetic response has been tuned when alkanethiol molecules (C18) bond to the SRRs (red line). (b) The control experiment with ethanol only is also shown. The DT signal is shown in the bottom of the panel with a blue line.

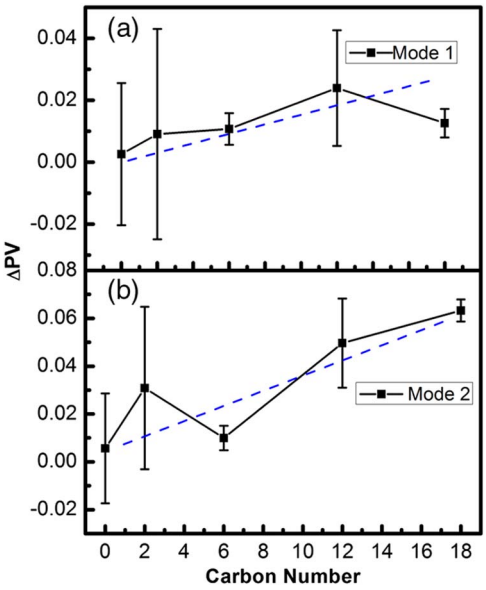

Fig. 6. (a) ΔPV change for Mode 1 when thiol molecules with different carbon atoms bond to metamaterials (carbon number 0 for control experiments with ethanol solution). (b) ΔPV change for Mode 2. The blue dash line is used to guide eyes.

1 near 0.4 THz and Mode 2 near 1.2 THz are observed, which are consistent with the simulation results. When alkanethiol molecules (C_{18}) are bond to metamaterials, the original data have been modulated as shown with the red line in Fig. 5(a). The pass band around 0.8 THz experiences a large attenuation when the molecule layer is deposited on the Au surfaces. This may arise from the molecule-induced surface impendence change of the metamaterials. The slight frequency shift and damping constant is evident from the resonant shape of the curve. Defining DT response as the differential change due to the binding of C_{18} thiol molecules, the DT signal is shown in the bottom panel. The enhanced DT response in the resonant region is observed and manifested in Fig. 5(a) by the arrow lines. The response at 1.2 THz (Mode 2) is more sensitive than Mode 1 at 0.4 THz, which could come from a different electromagnetic mechanism with different sensitivity and is consistent with the calculation in Fig. 2(a). However, Mode 1 could be potentially be more sensitive than Mode 2 when the SAM molecules were introduced in the gap region of the SRRs [31], which may change the capacitance and result in the great redshift for Mode 1. The control experiment about nonspecific interaction with metamaterials by dipping metamaterials into pure ethanol is conducted and the curve shapes are almost unchanged in resonant regions as shown in Fig. 5(b).

We further introduce the ΔPV value in the DT spectra to monitor the change of chain length of different alkanethiol molecules. The reaction of different thiol molecules with metamaterials are controlled in the same condition to ensure different thiol molecules covered metamaterial surfaces efficiently. Figure 6 shows the ΔPV signal of resonant modes when thiol molecules bearing different alkyl chain with different carbon atoms bond to metamaterials. Figure 6(a) is for Mode 1 and Fig. 6(b) is for Mode 2. The results suggest that the carbon-number-dependent tendency is approximately linear (blue dash lines in Fig. 6). The results are consistent with the experiments in the visible region, which suggests the wavelength linearly redshift 3 nm for every methylene (–CH_2–) in the alkyl chain [34]. It has to be mentioned that the C–C bond length is 1.54×10^{-10} m, and the thickness of the layers is on the scale of several nanometers. The sensing of these molecules with a THz wave would be challenging without the help of metamaterials. Compared with the visible region, the sensing in the THz region would mainly come from the intermolecular transition response instead of the variation of the electron state in the visible region. This method shows some advantage in comparison with conventional THz metamaterial sensing. For example, the frequency shift value would be inevitable for frequency shift interrogation, while the ΔPV still give a reasonable value. The results also show that the higher resonance mode is more sensitive to molecules than the lower one. The explanation on the mechanism would be attributed to the different origin of the two modes. As stated before, the lower resonance mode arises from the combination of the capacitance and inductance, while the higher one originates from the standing pattern along the length of the ring. The higher resonance mode could be enhanced resonantly to the bonded intra or intermolecular vibrations [26,31], resulting in its higher sensitivity compared with that for the lower resonant mode.

The molecular longitudinal axis is usually not along the surface normal direction of metamaterials but along a tilted angle of approximate 20°–35° [40], which is governed by the intermolecular interaction as well as the interaction of the dipole with the metamaterials [41]. The alkanethiol molecules form a monolayer of positive interface dipoles [40] and these

intersurface dipoles interact with the Au surface of metamaterials in the format of electron transfer and/or microenvironmental dielectric constant change, which introduces DT change and further ΔPV values near the resonant region. Usually, the dielectric constant variation mainly leads to the shift of f_c and Γ, while the electron transfer mainly brings the change of Γ. Frequency (wavelength) and intensity interrogations mainly capture frequency shift information. DT interrogation, however, in principle monitor both frequency shift and damping change information cooperatively, especially for the case as charge transfers between the substrate and the sensing molecules. Chemically modified metamaterials with the alkanethiol self-assembled monolayers have two effects on the metamaterials. First, the polarizability formed by the dipoles introduce the microenvironment variation on the metamaterial surface [42] from the vacuum dielectric constant ε_0 to an effective dielectric constant ε_{eff}. This mainly introduces the f_c change as demonstrated by others [43]. Second, the surface potential of the metamaterials is modified due to the Helmholtz potential formed by the self-assembled monolayer as follows [42]:

$$\Delta E_{\text{vac}}(n) = -\frac{en\mu_0}{\varepsilon_0\varepsilon_{\text{eff}}(n)}, \tag{3}$$

where e is the elementary charge, μ_0 is the dipole moment of the isolated molecules, and n is the area density of dipoles on the surface. The surface potential further introduces the electron transfer between molecules and metamaterials due to the energy level alignment [44], which results in the change of damping constant. As discussed above, ΔPV are also due to two aspects: one from the ε_{eff} and the other from the surface dipole-induced surface potential change.

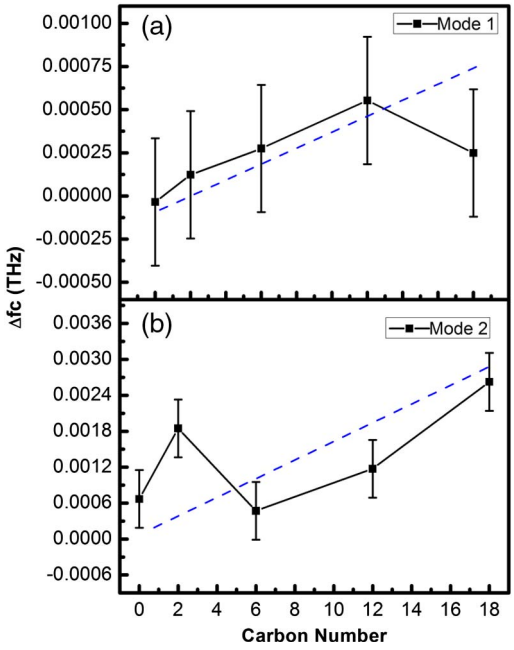

Fig. 7. (a) f_c change for Mode 1 when thiol molecules with different carbon atoms bond to metamaterials (carbon number 0 for control experiments with ethanol solution). (b) f_c change for Mode 2. The blue dash line is used to guide eyes.

For comparison, we also do Lorentz fittings for the resonant frequency changes due to different thiol molecules. The initial f_c for Mode1 and Mode 2 is about 0.420 and 1.232 THz for pristine metamaterials, respectively. The initial Γ for Mode 1 and Mode 2 is about 0.1080 and 0.2020 THz, respectively. The fittings suggest that the Γ change is almost constant with the value of approximate 0.0004 THz for all thiol molecules. Figure 7 demonstrates the f_c change for Mode1 [Fig. 7(a)] and Mode 2 [Fig. 7(b)] when thiol molecules with different carbon atoms bond to metamaterials. It is evident that the carbon number dependent with f_c change is approximately linear (blue dash lines in Fig. 7). This is consistent with ΔPV dependent with the carbon numbers in Fig. 6.

6. Conclusion

We have theoretically and experimentally demonstrated that DT can capture both the frequency shift and the damping constant change cooperatively in the application of THz metamaterial sensing. The enhanced THz response near resonant regions in metamaterials offers a promising way to read out the carbon number in the self-assembled alkanethiol molecular monolayers. Surface dipoles formed by alkanethiol molecules interact with metamaterials in the format of electron transfer and/or microenvironmental dielectric constant change, which mainly introduces DT change near the resonant region. Numerical simulations also confirm that the enhancement is large at the gap and corner regions of this kind of metamaterials. Our results can be extended to other wavelength regions and can be used for other shapes of metamaterials analysis as well.

This work is supported by the National Natural Science Foundation of China (Grant Nos. 10834015, 51103175, and 61077082), the National Basic Research Program of China (Grant No. 2009CB930502), the Natural Science Basic Research Plan in Shaanxi Province of China (Program No. 2012KJXX-27), and the Knowledge Innovation Project of CAS (Grant No. KJCX2-EW-W02).

References

1. J. Homola, S. S. Yee, and G. Gauglitz, "Surface plasmon resonance sensors: review," Sens. Actuators B **54**, 3–15 (1999).
2. K. A. Willets and R. P. Van Duyne, "Localized surface plasmon resonance spectroscopy and sensing," Annu. Rev. Phys. Chem. **58**, 267–297 (2007).
3. D. R. Smith, J. B. Pendry, and M. C. K. Wiltshire, "Metamaterials and negative refractive index," Science **305**, 788–792 (2004).
4. Z. Jakšić, O. Jakšić, Z. Djurić, and C. Kment, "A consideration of the use of metamaterials for sensing applications: field fluctuations and ultimate performance," J. Opt. A **9**, S377–S384 (2007).
5. C. Jeppesen, S. Xiao, N. A. Mortensen, and A. Kristensen, "Metamaterial localized resonance sensors: prospects and limitations," Opt. Express **18**, 25075–25080 (2010).

6. N. I. Zheludev, "The road ahead for metamaterials," Science **328**, 582–583 (2010).
7. X. J. Wu, X. C. Pan, B. G. Quan, X. L. Xu, C. Z. Gu, and L. Wang, "Self-referenced sensing based on terahertz metamaterial for aqueous solutions," Appl. Phys. Lett. **102**, 151109 (2013).
8. X. J. Wu, B. G. Quan, X. C. Pan, X. L. Xu, X. C. Lu, C. Z. Gu, and L. Wang, "Alkanethiol-functionalized terahertz metamaterial as label-free, highly-sensitive and specific biosensor," Biosens. Bioelectron. **42**, 626–631 (2013).
9. I. A. I. Al-Naib, C. Jansen, and M. Koch, "Thin-film sensing with planar asymmetric metamaterial resonators," Appl. Phys. Lett. **93**, 083507 (2008).
10. C. Debus and P. H. Bolivar, "Frequency selective surfaces for high sensitivity terahertz sensing," Appl. Phys. Lett. **91**, 184102 (2007).
11. H. J. Lee, K. H. Yoo, and J. G. Yook, "DNA sensing using split-ring resonator alone at microwave Regime," J. Appl. Phys. **108**, 014908 (2010).
12. Y. Sun, X. Xia, H. Feng, H. Yang, C. Gu, and L. Wang, "Modulated terahertz responses of split ring resonators by nanometer thick liquid layers," Appl. Phys. Lett. **92**, 221101 (2008).
13. X. L. Xu, B. Peng, D. Li, J. Zhang, L. M. Wong, Q. Zhang, S. J. Wang, and Q. H. Xiong, "Flexible visible-infrared metamaterials and their applications in highly sensitive chemical and biological sensing," Nano Lett. **11**, 3232–3238 (2011).
14. Y.-T. Chang, Y.-C. Lai, C.-T. Li, C.-K. Chen, and T.-J. Yen, "A multi-functional plasmonic biosensor," Opt. Express **18**, 9561–9569 (2010).
15. B. Lahiri, A. Z. Khokhar, R. M. De La Rue, S. G. McMeekin, and N. P. Johnson, "Asymmetric split ring resonators for optical sensing of organic materials," Opt. Express **17**, 1107–1115 (2009).
16. H. Aouani, H. Sipova, M. Rahmani, M. Navarro-Cia, K. Hegnerova, J. Homola, M. H. Hong, and S. A. Maier, "Ultrasensitive broadband probing of molecular vibrational modes with multifrequency optical antennas," ACS Nano **7**, 669–675 (2013).
17. M. Navarro-Cia, M. Beruete, S. Agrafiotis, F. Falcone, M. Sorolla, and S. A. Maier, "Broadband spoof plasmons and subwavelength electromagnetic energy confinement on ultrathin metafilms," Opt. Express **17**, 18184–18195 (2009).
18. G. Kumar, A. Cui, S. Pandey, and A. Nahata, "Planar terahertz waveguides based on complementary split ring resonators," Opt. Express **19**, 1072–1080 (2011).
19. H.-J. Lee and J.-G. Yook, "Biosensing using split-ring resonators at microwave regime," Appl. Phys. Lett. **92**, 254103 (2008).
20. H. Yoshida, Y. Ogawa, Y. Kawai, S. Hayashi, A. Hayashi, C. Otani, E. Kato, F. Miyamaru, and K. Kawase, "Terahertz sensing method for protein detection using a thin metallic mesh," Appl. Phys. Lett. **91**, 253901 (2007).
21. T. Driscoll, G. O. Andreev, D. N. Basov, S. Palit, S. Y. Cho, N. M. Jokerst, and D. R. Smith, "Tuned permeability in terahertz split-ring resonators for devices and sensors," Appl. Phys. Lett. **91**, 062511 (2007).
22. H. Tao, L. R. Chieffo, M. A. Brenckle, S. M. Siebert, M. Liu, A. C. Strikwerda, K. B. Fan, D. L. Kaplan, X. Zhang, R. D. Averitt, and F. G. Omenetto, "Metamaterials on paper as a sensing platform," Adv. Mater. **23**, 3197–3201 (2011).
23. S.-Y. Chiam, R. Singh, J. Q. Gu, J. G. Han, W. L. Zhang, and A. A. Bettiol, "Increased frequency shifts in high aspect ratio terahertz split ring resonators," Appl. Phys. Lett. **94**, 064102 (2009).
24. S.-Y. Chiam, R. Singh, W. L. Zhang, and A. A. Bettiol, "Controlling metamaterial resonances via dielectric and aspect ratio effects," Appl. Phys. Lett. **97**, 191906 (2010).
25. J. F. O'Hara, R. Singh, I. Brener, E. Smirnova, J. G. Han, A. J. Taylor, and W. L. Zhang, "Thin-film sensing with planar terahertz metamaterials: sensitivity and limitations," Opt. Express **16**, 1786–1795 (2008).
26. C. Wu, A. B. Khanikaev, R. Adato, N. Arju, A. A. Yanik, H. Altug, and G. Shvets, "Fano-resonant asymmetric metamaterials for ultrasensitive spectroscopy and identification of molecular monolayers," Nat. Mater. **11**, 69–75 (2012).
27. W. Cao, R. Singh, I. A. I. Al-Naib, M. X. He, A. J. Taylor, and W. L. Zhang, "Low-loss ultra-high-Q dark mode plasmonic Fano metamaterials," Opt. Lett. **37**, 3366–3368 (2012).
28. R. Singh, I. A. I. Al-Naib, Y. P. Yang, D. R. Chowdhury, W. Cao, C. Rockstuhl, T. Ozaki, R. Morandotti, and W. L. Zhang, "Observing metamaterial induced transparency in individual Fano resonators with broken symmetry," Appl. Phys. Lett. **99**, 201107 (2011).
29. R. Singh, I. A. I. Al-Naib, M. Koch, and W. L. Zhang, "Sharp Fano resonances in THz metamaterials," Opt. Express **19**, 6312–6319 (2011).
30. X. Xia, Y. Sun, H. Yang, H. Feng, L. Wang, and C. Gu, "The influences of substrate and metal properties on the magnetic response of metamaterials at terahertz region," J. Appl. Phys. **104**, 033505 (2008).
31. E. Cubukcu, S. Zhang, Y. S. Park, G. Bartal, and X. Zhang, "Split ring resonator sensors for infrared detection of single molecular monolayers," Appl. Phys. Lett. **95**, 043113 (2009).
32. X. L. Xu, B. G. Quan, C. Z. Gu, and L. Wang, "Bianisotropic response of microfabricated metamaterials in the terahertz region," J. Opt. Soc. Am. B **23**, 1174–1180 (2006).
33. X. P. Zhang, X. W. Ma, F. Dou, P. X. Zhao, and H. M. Liu, "A biosensor based on metallic photonic crystals for the detection of specific bioreactions," Adv. Funct. Mater. **21**, 4219–4227 (2011).
34. M. D. Malinsky, K. L. Kelly, G. C. Schatz, and R. P. Van Duyne, "Chain length dependence and sensing capabilities of the localized surface plasmon resonance of silver nanoparticles chemically modified with alkanethiol self-assembled monolayers," J. Am. Chem. Soc. **123**, 1471–1482 (2001).
35. H. B. Akkerman, P. W. M. Blom, D. M. De Leeuw, and B. De Boer, "Towards molecular electronics with large-area molecular junctions," Nature **441**, 69–72 (2006).
36. G. M. Whitesides, E. Ostuni, S. Takayama, X. Jiang, and D. E. Ingber, "Soft lithography in biology and biochemistry," Annu. Rev. Biomed. Eng. **3**, 335–373 (2001).
37. L. S. Jung and C. T. Campbell, "Sticking probabilities in adsorption from liquid solutions: alkylthiols on gold," Phys. Rev. Lett. **84**, 5164–5167 (2000).
38. U. MØller, J. R. Folkenberg, and P. U. Jepsen, "Dielectric properties of water in butter and water–AOT–heptane systems measured using terahertz time-domain spectroscopy," Appl. Spectrosc. **64**, 1028–1036 (2010).
39. B. G. Quan, X. L. Xu, H. F. Yang, X. X. Xia, Q. Wang, L. Wang, C. Z. Gu, C. Li, and F. Li, "Time-resolved broadband analysis of split ring resonators in terahertz region," Appl. Phys. Lett. **89**, 041101 (2006).
40. D. M. Alloway, M. Hofmann, D. L. Smith, N. E. Gruhn, A. L. Graham, R. Colorado, Jr., V. H. Vysocki, T. R. Lee, P. A. Lee, and N. R. Armstrong, "Interface dipoles arising from self-assembled monolayers on gold: UV-photoemission studies of alkanethiols and partially fluorinated alkanethiols," J. Phys. Chem. B **107**, 11690–11699 (2003).
41. C.-X. Wu and M. Iwamoto, "Calculation of the dielectric constant of monolayer films with dielectric anisotropy," Phys. Rev. B **55**, 10922–10930 (1997).
42. L. Romaner, G. Heimel, C. Ambrosch-Draxl, and E. Zojer, "The dielectric constant of self-assembled monolayers," Adv. Funct. Mater. **18**, 3999–4006 (2008).
43. Z. Tian, J. Han, X. Lu, J. Gu, Q. Xing, and W. Zhang, "Surface plasmon enhanced terahertz spectroscopic distinguishing between isotopes," Chem. Phys. Lett. **475**, 132–134 (2009).
44. M. Knupfer and G. Paasch, "Origin of the interface dipole at interfaces between undoped organic semiconductors and metals," J. Vac. Sci. Technol. A **23**, 1072–1077 (2005).